Entanglement from the Diósi–Penrose Model: An Exact Criterion, and Why It Stays Small at Any Distance

Marc Sperzel*

Independent Researcher

November 11, 2026

Abstract

Trillo and Navascués showed that the Diósi–Penrose model, in the Tilloy–Diósi form with the same smearing length σ in force and noise, entangles two masses in superposition when they are closer than about $2.2\,\sigma$, and asked whether gravitationally induced entanglement can be observed beyond that distance. We answer for two rigid bodies whose branches are position eigenstates on finite sets, without kinetic term, for noise strength C. One kernel, the Coulomb energy of the smeared bodies, sets both the Newtonian coupling and the correlated noise, and the question becomes a single geometric comparison: a product state becomes entangled if and only if the largest canonical correlation between neutral charge patterns on the two branch sets exceeds $C/\sqrt{1+C^2}$. Below this threshold the evolution is a separable operation at all times. The published critical distances are two-branch cases of the criterion: for parallel two-branch superpositions the supremum is $2.21\,\sigma$ at $C=1$, and a straddling geometry reaches $2.74\,\sigma$. With many branches there is no critical distance. What limits the effect is the model's own dephasing, which sits in the same quadratic form. For bodies of effective size σ_{eff} (σ for point masses) separated by a slab of width $d \gg \sigma$, the entangling rate at $C=1$ is at most $0.12\,\sigma_{\mathrm{eff}}/d$ times the single-body dephasing rate, to leading order in σ/d. For branches more than σ_{eff} apart the entanglement is therefore transient and, if well separated, a fraction of order σ_{eff}/d of what unitary Newtonian gravity gives; below σ it can last for days. Entanglement of the size unitary gravity predicts still excludes the model; the inference from any detected entanglement beyond a fixed multiple of σ does not hold.

Contents

1 Introduction . . . 2
2 The idea: one kernel, one comparison . . . 3
3 The model and the criterion . . . 5
4 Two-branch states, and why many branches have no critical distance . . . 7
5 The entangling rate against the model's own dephasing . . . 9
6 The Bose *et al.* design and the inference from an observation . . . 12
7 Scope and discussion . . . 13
A Proof of the separable half, and wavefunctions . . . 14
B Proofs of the bounds . . . 16
C Numerical values . . . 18

*ORCID: 0009-0000-6252-3155. Email: me@marcsperzel.com

1 Introduction

The question

If gravity is a quantum channel, two masses that are each in a superposition of positions become entangled through their gravitational interaction, and the detection of that entanglement has been proposed as a witness of the quantum nature of gravity [1, 2]. The witness needs a classical benchmark. The Diósi–Penrose model [3, 4, 5], in the form of Tilloy and Diósi [6, 7], is one. Its Newtonian field is sourced by continuously monitored mass densities, smeared over a length σ, and the monitoring dephases superpositions of position, a decoherence that the positivity of the dynamics forces [8]. Trillo and Navascués showed that this model nevertheless entangles two masses, in the same geometries in which the quantum prediction is made [9]. For two branches per mass they found critical distances d_c, about $0.85\,\sigma$ for collinear superpositions of vanishing size and $2.21\,\sigma$ for transversal superpositions of diverging size, and asked: "Is there a way to observe GIE [gravitationally induced entanglement] beyond d_c?" We answer in the form: for which states does the model entangle two masses, and how much?

Why it was open

Later work quotes $d_c \approx 0.85\,\sigma$ as the separation below which the model entangles [10, 11]. That is correct for small packets with two branches; nothing was known for more. Wang, Pedernales and Plenio, in a study of local error correction, gave a separability lemma for one pair of coupled operators, found the Diósi–Penrose dynamics of their two-level codes separable outside a small region of d/σ, and left the exact classification as "beyond our scope" [12]. With more than two branches per mass several operators are coupled at once, and a condition on each pair does not in general give a condition on the whole. An exact answer needs a structure that decouples them.

The answer

The structure exists. The model uses one kernel, the Coulomb energy between smeared mass distributions, three times: for the Newtonian coupling of the two bodies, for the noise that is correlated between them, and for the dephasing of each body by itself. With no kinetic term, two rigid bodies in a product state on finite sets of position branches therefore become entangled if and only if

$$\rho_{\max}(S_A, S_B) \;>\; \frac{C}{\sqrt{1+C^2}}, \tag{1}$$

where $\rho_{\max}$ is the largest canonical correlation [13] between neutral charge patterns on the two branch sets, the cosine of the smallest angle between them with the Coulomb energy as inner product, and $C \geq 1$ is the noise strength ($C = 1$ in [9]). Below the threshold the evolution is a separable operation for all time (Theorem 3.2).

Two branches per body give one pattern each, and the published critical distances follow. Many branches give each body a space of patterns, and two such spaces can be aligned at any separation: the model has no critical distance. What it has is a limit on the size of the entanglement, which is produced at a rate Γ_{ent} that is a small fraction of the rate Γ_{sat} at which

the same dynamics dephases each body,

$$\frac{\Gamma_{\text{ent}}}{\Gamma_{\text{sat}}} \;=\; \frac{\sqrt{\pi}\,\kappa}{C}\,\frac{\sigma_{\text{eff}}}{d} \;\le\; 0.12\,\frac{\sigma_{\text{eff}}}{d} \qquad (C=1,\ \text{slab-separated supports},\ \sigma \ll d). \tag{2}$$

Here κ is a dimensionless rate constant, d the width of a slab that separates the branches of the two bodies, $\Gamma_{\text{sat}} = C\,Gm^2/(\sqrt{\pi}\,\hbar\,\sigma_{\text{eff}})$ the saturated Diósi–Penrose dephasing rate, and σ_{eff} the effective size of a smeared body ($\sigma_{\text{eff}} = \sigma$ for point masses). The bound is the leading order in σ/d; for planar supports the coefficient is 0.13 at $d = 10\,\sigma$ and 0.18 at $d = 3\,\sigma$. When the branches of each body are further apart than σ_{eff}, the entanglement therefore peaks at about $\Gamma_{\text{ent}}/(2e\Gamma_{\text{sat}})$, half a dephasing time after preparation, and then decays. Superpositions smaller than σ dephase more slowly, and there the entanglement can survive for more than a day, as Trillo and Navascués found [9]. For the design of Bose *et al.* [1] at $C = 1$ the two-branch state is entangled only if $\sigma > 524$ μm, and for σ below the radius of the masses the best many-branch state known entangles at 8.6×10^{-3} s^{-1} while each mass dephases at 86 s^{-1}.

What is not shown

The "if and only if" is a statement about position-eigenstate branches. For wavefunctions whose support has interior the canonical correlation is one, and we give no bound on what wavepackets of finite width produce. Beyond the initial rate, all results are for a vanishing kinetic term. The preparation of a many-branch state, during which the same dephasing acts, is not modelled. The law for the size of the entanglement is derived at leading order without an error bound; the proven bound needs many branches, more than a few σ apart. The two-branch optimum over all geometries rests on a numerical search and a computer-assisted ceiling, and the best rate constant is bracketed, not determined. Section 7 gives the full scope.

2 The idea: one kernel, one comparison

In the Diósi–Penrose model the pull between two bodies and the noise that decoheres them are one quantity, the Coulomb energy $\langle u, v\rangle = \iint u(x)v(y)/|x-y|$ between smeared mass distributions. Entanglement then becomes a matter of one angle against one number.

One kernel. In the master equation, Eq. (4), the Newtonian interaction and the monitoring noise integrate the same smeared mass density against the same kernel $1/|x-y|$. On position branches a coherence sees only the difference of two mass distributions. For one body with branches a, a' this is a dipole: the smeared body at a, minus the smeared body at a'. Let u and v be such dipoles of bodies A and B, weighted by the masses. With no kinetic term, the coherence between the configurations ab and $a'b'$ acquires the Newtonian phase and decays at a rate proportional to $C\,\|u+v\|^2 = C\,(\|u\|^2 + \|v\|^2 + 2\langle u, v\rangle)$, with $\|u\|^2 = \langle u, u\rangle$ (Eq. (7)). The norms dephase each body by itself, at the Diósi–Penrose rate; the cross term is noise correlated between the bodies; the Newtonian phase is the same Coulomb energy, evaluated between them. A classical field that pushes two bodies must also decohere them [8]; here push and decoherence are one bilinear form.

One comparison. Entanglement first appears as a negative eigenvalue of the partial transpose. Its witness reads a neutral pattern q_1 on the branches of A, a combination of such dipoles, and

a pattern q_2 on those of B. At first order in time the eigenvalue has the sign of

$$C\,\|q_1\|^2 + C\,\|q_2\|^2 - 2\,\mathrm{Re}\big[(C+i)\langle q_1, q_2\rangle\big]. \tag{3}$$

The first two terms are the cost, the dephasing of the collective coherences that the witness reads. The last is the gain: the force supplies the i, the correlated noise the C, and with the best relative phase it is $2\sqrt{1+C^2}\,|\langle q_1, q_2\rangle|$. Cost and gain are measured in one metric, so their comparison is an angle: with the best relative scale the form is negative if and only if the cosine $|\langle q_1, q_2\rangle|/(\|q_1\|\|q_2\|)$ exceeds $C/\sqrt{1+C^2}$. Masses, amplitudes and time do not enter. Noise alone would put the threshold at one, which no cosine exceeds; the force brings it down, to $1/\sqrt{2}$ at $C = 1$. The patterns always split into pairs of directions, one on each body, that couple to no other pair; below the threshold the evolution on each pair is a mixture of local operations, and the state stays separable for all time.

Two branches: one dipole each. With two branches a body has a single pattern, so the geometry fixes the angle. For two long dipoles side by side at distance d, each end faces the like end of the other: the mutual energy is that of two smeared points at distance d, the self-energy that of one, and the cosine is their ratio, $\sqrt{\pi}\,\sigma\,\mathrm{erf}(d/2\sigma)/d$, which falls below $1/\sqrt{2}$ at $d = 2.21\,\sigma$. Other geometries change the number, not the conclusion: one fixed direction per body is aligned with the other only within a few σ. These are the critical distances of [9].

Many branches: a condenser. With many branches each body has a space of patterns, and two spaces can contain nearly parallel vectors where two given vectors do not. Spread the branches of A over a disc of radius a, those of B over the same disc displaced by the gap d, and give both the same uniform charge. Their difference is a charged parallel-plate condenser, whose field is confined to the gap: its energy is smaller than the self-energy of one plate by a factor of order d/a, and the cosine is one minus a term of that order. Discs several gaps wide carry nearly parallel patterns, however large d/σ is. (A distant copy of each disc with the opposite charge, the two copies facing each other at the same gap d, makes the patterns neutral; the self-energies of the single smeared points enter divided by the number of branches.) There is no critical distance.

Why the entanglement stays small. The form (3) fixes the size as well as the sign. Its gain is a Newtonian energy at distance d, so the negative eigenvalue grows at a rate Γ_{ent} of order $Gm^2/(\hbar d)$ at most. Meanwhile each pair of branches of one body dephases at a rate set by the body's own self-energy, which saturates for a rigid body: two positions further apart than the effective size σ_{eff} of the smeared body dephase at $\Gamma_{\mathrm{sat}} = CGm^2/(\sqrt{\pi}\,\hbar\,\sigma_{\mathrm{eff}})$, however far apart they are. Many branches dilute the self-energy of the pattern that the witness reads, which is how they make the sign negative; they do not dilute the dephasing of the state that carries it. At leading order, for many branches, $\lambda_{\min}(t) \simeq -\Gamma_{\mathrm{ent}}\,t\,e^{-2\Gamma_{\mathrm{sat}}t}$, with one factor $e^{-\Gamma_{\mathrm{sat}}t}$ for the coherence on each body and $\Gamma_{\mathrm{ent}}/\Gamma_{\mathrm{sat}} = O(\sigma_{\mathrm{eff}}/d)$. The entanglement grows for half a dephasing time, peaks at $\Gamma_{\mathrm{ent}}/(2e\Gamma_{\mathrm{sat}})$, and decays.

3 The model and the criterion

3.1 The master equation in the position basis

The Tilloy–Diósi dynamics with smeared force and noise, in the notation of [9] with a noise strength C, is

$$\dot\rho = -\frac{i}{\hbar}[H,\rho] + \frac{G}{2\hbar}\iint \frac{d^3r\,d^3s}{|\mathbf{r}-\mathbf{s}|}\Big(- C\,[\mu_\sigma(\mathbf{r}),[\mu_\sigma(\mathbf{s}),\rho]] + i\,[\mu_\sigma(\mathbf{r})\mu_\sigma(\mathbf{s}),\rho]\Big), \tag{4}$$

with μ_σ the mass density smeared by a normalised Gaussian of standard deviation σ. The second term is the Newtonian interaction of the smeared densities, the first the monitoring noise; both carry the same density and the same kernel. In measurement-and-feedback realisations $C \geq 1$, and $C = 1$ is the least-decoherence point [6, 7], the case of [9].

Two rigid bodies A, B with masses m_A, m_B carry their centres as quantum degrees of freedom. Let g_a be the σ-smeared unit-mass density of body A centred at a, and g_b that of B. On charge densities use the Coulomb form $\langle u, v\rangle = \iint u(x)v(y)/|x-y|$ and put

$$f_A(a,a') = \langle g_a, g_{a'}\rangle, \qquad f_B(b,b') = \langle g_b, g_{b'}\rangle, \qquad F(a,b) = \langle g_a, g_b\rangle. \tag{5}$$

For point masses all three equal $f(r) = \operatorname{erf}(r/2\sigma)/r$, with $f(0) = f_0 = 1/(\sqrt{\pi}\,\sigma)$. With $H = 0$, Eq. (4) acts on position matrix elements multiplicatively,

$$\rho_t(ab,a'b') = \rho_0(ab,a'b')\,\exp\Big[\frac{Gt}{\hbar}\,\Lambda(ab,a'b')\Big], \tag{6}$$

$$\Lambda = i\,m_Am_B\big[F(a,b) - F(a',b')\big] - \frac{C}{2}\,\big\|m_A(g_a - g_{a'}) + m_B(g_b - g_{b'})\big\|^2. \tag{7}$$

The norm is the Coulomb norm, $\|u\|^2 = \langle u, u\rangle$. Expanded, the real part is $-C\,[m_A^2 D_A + m_B^2 D_B + m_Am_B\,\delta]$ with $D_A = f_A(a,a) - f_A(a,a')$, D_B likewise, and $\delta = F(a,b) + F(a',b') - F(a,b') - F(a',b)$. The local terms D_A, D_B are the Diósi–Penrose dephasing of each body; δ is the correlated part of the noise.

3.2 The criterion

A state is a *branch state* on finite sets S_A, S_B of centre positions if it is supported on $S_A \times S_B$; for a product state $\psi_A \otimes \psi_B$ write $p_a = |\psi_A(a)|^2$, $r_b = |\psi_B(b)|^2$. The branches are position eigenstates (Section 7 discusses wavepackets). We use two measures of separation: the *closest approach*, the smallest distance between a branch of A and a branch of B; and the *slab separation* d, for which some plane has all branches of A on one side and all branches of B on the other, at normal distance at least d. The second implies the first and forbids one body from sitting between the branches of the other.

Definition 3.1. Let $V_A = \operatorname{span}\{g_a - g_{a'} : a, a' \in S_A\}$ and V_B likewise: the neutral charge patterns on the branch sets. Their largest Coulomb canonical correlation is

$$\rho_{\max}(S_A,S_B) = \sup\Big\{\frac{|\langle u,v\rangle|}{\|u\|\,\|v\|} :\ u \in V_A,\ v \in V_B\Big\}, \qquad s_*(C) = \frac{C}{\sqrt{1+C^2}}. \tag{8}$$

$\rho_{\max}$ is the cosine of the smallest angle between V_A and V_B: the top singular value of

$f_A^{-1/2} F f_B^{-1/2}$ restricted to zero-sum vectors. It does not depend on the masses. $s_*(1) = 1/\sqrt{2} = 0.7071$. The theorem says that these two numbers decide the question, in both directions and for all times.

Theorem 3.2 (Entanglement criterion)**.** *Let $H = 0$ and $C > 0$, and let S_A, S_B be finite sets of distinct branches.*

(a) If $\rho_{\max} > s_*$, every pure product state with all amplitudes non-zero has a partial transpose with a negative eigenvalue for all sufficiently small $t > 0$. That eigenvalue leaves zero at the rate

$$\dot{\lambda} = \frac{G}{\hbar} \min_{q_1, q_2} \frac{C m_A^2 \langle q_1, q_1\rangle + C m_B^2 \langle q_2, q_2\rangle - 2 m_A m_B \,\mathrm{Re}[(C+i)\langle q_1, q_2\rangle]}{\sum_a |q_1(a)|^2/p_a + \sum_b |q_2(b)|^2/r_b}, \tag{9}$$

the minimum over neutral complex patterns q_1 on S_A and q_2 on S_B, with $\langle q_1, q_2\rangle = \sum_{ab} \bar{q}_1(a) q_2(b) F(a,b)$ and $\langle q_1, q_1\rangle = \sum \bar{q}_1(a) q_1(a') f_A(a,a')$.

(b) If $\rho_{\max} \le s_*$, the evolution restricted to $S_A \times S_B$ is a separable operation for every $t \ge 0$: a mixture of products of local completely positive maps. Every separable initial state stays separable, also when local channels acting within the branch spaces are interleaved.

(c) Hence the model entangles some product state on $S_A \times S_B$ at some time if and only if it entangles every full-support pure product state at first order, if and only if $\rho_{\max} > s_*$.

Proof sketch. (a) Partial transposition, written T_1, exchanges $a \leftrightarrow a'$, and $\rho_0^{T_1}$ is a rank-one projector. For a vector χ orthogonal to it put $c = \tilde{\Psi}^* \chi$ entrywise, $\tilde{\Psi} = \bar{\psi}_A \otimes \psi_B$, so that $\sum c = 0$. At first order in t every term of Λ that depends on (a,b) alone or on (a',b') alone drops out of $\langle \chi | \rho_t^{T_1} | \chi \rangle$, and with the marginals $q_1(a) = \sum_b c(ab)$, $q_2(b) = \sum_a c(ab)$ what remains is the numerator of Eq. (9). Every pair of neutral patterns arises, through $c = q_1 \otimes r + p \otimes q_2$, which also minimises $\|\chi\|^2$ at given marginals and gives the denominator. Optimising the phase and the scale of q_2, the numerator is negative for some pair if and only if $|\langle q_1, q_2\rangle|^2 > s_*^2 \langle q_1, q_1\rangle \langle q_2, q_2\rangle$, that is, if and only if $\rho_{\max} > s_*$; the state is then entangled by the Peres criterion [14].

(b) Choose bases of V_A and V_B that diagonalise the cross form (a singular value decomposition with singular values $s_i \le \rho_{\max}$) and let $x_i(a)$, $y_i(b)$ be the coordinates of the branches in them. Since one kernel F enters both the force and the correlated noise, and the local dephasing is the Gram form used for the whitening,

$$\begin{aligned} \Lambda &= \sum_i \Lambda_i + (\text{local phases}), \\ \Lambda_i &= i s_i (x_i y_i - x_i' y_i') - \tfrac{C}{2}(x_i - x_i')^2 - \tfrac{C}{2}(y_i - y_i')^2 - C s_i (x_i - x_i')(y_i - y_i'), \end{aligned} \tag{10}$$

with no terms coupling different i (masses absorbed into g). Each Λ_i is reproduced by random local phase-and-amplitude multipliers $e^{x_i(\eta_i + i\zeta_i)}$, $e^{y_i(\eta_i' + i\zeta_i')}$ with Gaussian latent variables, up to a local Schur multiplier with exponent $t\,(C - s_i\sqrt{1+C^2})\, x_i x_i'$. When $s_i\sqrt{1+C^2} \le C$ for every i that multiplier is positive semidefinite, hence completely positive, and ρ_t is an average of products of local completely positive maps applied to ρ_0. Appendix A gives the covariance and the bookkeeping. (c) follows from (a) and (b). □

The criterion depends on the branch sets, σ, the shapes of the bodies and C, not on the masses, the amplitudes or the time. A pair of patterns (q_1, q_2) that makes the numerator of

Eq. (9) negative is called a *witness*. The threshold is below one because $|C+i| = \sqrt{1+C^2} > C$. Mode by mode the generator is never positive (for one Fourier mode the two-by-two form has determinant $C^2 - (1+C^2) = -1$), so separability comes only from the two bodies occupying different regions.

Remark 3.1 (Generality). The proof uses only that one real cross kernel enters both the Hamiltonian and the correlated noise and that the local dephasing is the Gram form. Theorem 3.2 therefore holds for any real cross kernel $\bar{F}$ with $\rho_{\max}$ replaced by the top singular value of $f_A^{-1/2}\bar{F}f_B^{-1/2}$ on neutral vectors, provided that value is at most one (otherwise the noise is not positive). Theorem 5.2 below uses this for $\bar{F} = \theta F$.

Remark 3.2 (Relation to Wang, Pedernales and Plenio). Each Λ_i in Eq. (10) is a generator of the form treated in Lemma 3 of [12], and their condition for $e^{t\Lambda_i}$ to be separable is $s_i\sqrt{1+C^2} \le C$ (Appendix A gives the dictionary). Part (b) therefore also follows from their lemma applied pair by pair, for one reason: the canonical decomposition leaves no cross terms between pairs, so $e^{t\Lambda}$ is a product of separable channels up to a local unitary. For several coupled operators a pairwise condition does not in general give a joint one (cf. their Theorem 1). With an unsmeared force, force and noise have different kernels, no single decomposition diagonalises both, and the pairwise argument fails for three or more branches. Necessity is part (a).

Remark 3.3 (The idealisation). Potentials of smeared charges are real-analytic, so the smeared point charges of any open set span the whole Coulomb space: $\rho_{\max} = 1$ for any two supports with interior. Every pair of wavefunctions whose supports have interior is therefore entangled at once, at every separation (Theorem A.1). The "if and only if" of Theorem 3.2 is a statement about position-eigenstate branches, the idealisation also used in [9, 12]. The physical content lies in the rate and the size of the entanglement, Section 5.

4 Two-branch states, and why many branches have no critical distance

4.1 The published distances as special cases

With two branches per body each space of patterns is a single dipole, and the canonical correlation is the cosine between the two dipoles. For $S_A = \{a_1, a_2\}$, $S_B = \{b_1, b_2\}$, Eq. (8) is

$$s = \frac{|f(a_1b_1) + f(a_2b_2) - f(a_1b_2) - f(a_2b_1)|}{2\sqrt{D(L_A)D(L_B)}}, \qquad D(L) = f_0 - f(L), \tag{11}$$

with $L_A = |a_1 - a_2|$, $L_B = |b_1 - b_2|$ and $f(xy) = f(|x-y|)$ (point masses). The cosine depends on how the dipoles are placed, so a critical distance belongs to a geometry and not to the model. Four limiting families have closed forms (Table 1, Fig. 1): superpositions of length $L \to 0$ along the line joining the bodies (collinear); superpositions perpendicular to that line (transversal), for $L \to 0$ and for $L \to \infty$; and a vanishing superposition of A midway between two branches of B, each at distance d (straddle). At their critical distances the collinear and straddle limits ($L \to 0$) and the transversal limit $L \to \infty$ are the suprema of s over L in their families, approached and not attained; s is not monotone in L for the collinear and straddle families. In the transversal family s increases with L, so the $L \to 0$ value is an infimum: below $1.547\,\sigma$ every transversal pair is entangled, between $1.547\,\sigma$ and $2.211\,\sigma$ only those with L above a d-dependent length

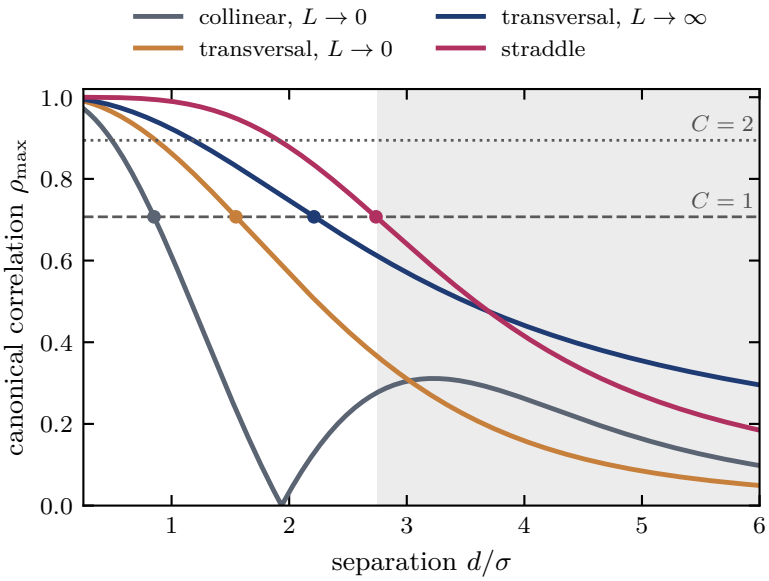


Figure 1. *Canonical correlation of the four limiting two-branch families against the separation, with the thresholds $s_*(1)$ and $s_*(2)$; dots mark the critical distances at $C = 1$. In the shaded region ($d \geq 2.75\,\sigma$ at slab separation) no two-branch state of any geometry is entangled at $C \geq 1$ (Proposition 4.2).*

($L > 2.12\,\sigma$ at $d = 1.6\,\sigma$). Setting the limits equal to s_* reproduces the two distances of [9] and adds two. For every $C \geq 1$ the straddle family has the largest critical distance of the four (Table 3 gives the dependence on C).

Table 1. *The four limiting two-branch families: the limit of the correlation s, with $\kappa_0 = -f''(0) = 1/(6\sqrt{\pi}\,\sigma^3)$ and $f(d)/f_0 = \sqrt{\pi}\,\sigma\,\mathrm{erf}(d/2\sigma)/d$, and the critical distance at $C = 1$, where the limit equals $s_*(1)$; d is the closest approach.*

family	limit of s	critical d/σ
collinear, $L \to 0$ [9]	$\lvert f''(d)\rvert/\kappa_0$	0.850872
transversal, $L \to 0$ (infimum over L)	$\lvert f'(d)/d\rvert/\kappa_0$	1.547134
transversal, $L \to \infty$ [9]	$f(d)/f_0$	2.210928
straddle	$\sqrt{2}\lvert f'(d)\rvert/\sqrt{\kappa_0(f_0 - f(2d))}$	2.738073

Most designs give both masses the same superposition, translated; the design of [1] is one. For this parallel class the transversal limit is the supremum.

Theorem 4.1 (Parallel superpositions)**.** *Let $S_A = \{a, a + w\}$ and $S_B = \{a + r, a + r + w\}$ for arbitrary vectors w, r, and let d be the closest approach. Then*

$$s \leq \max\left(f(d)/f_0,\ c_*\right), \qquad c_* = \Lambda_+ L_{1/2}^2/f_0 \approx 0.635, \tag{12}$$

where $\Lambda_+ = \max f''$ and $f(L_{1/2}) = f_0/2$ (values in Table 2). For every C with $s_*(C) \geq c_*$, in particular every $C \geq 1$, no parallel two-branch state with closest approach $d \geq d_*(C)$ is entangled, where $f(d_*)/f_0 = s_*(C)$ ($d_* = 2.21\,\sigma$ at $C = 1$); for every $d < d_*(C)$ some are.

Within the parallel class, then, the model entangles at $C = 1$ only below $2.21\,\sigma$, a supremum that long transversal superpositions approach and no state attains. The proof (Appendix B) uses that $h(x) = f(\sqrt{x})$ is a mixture of decaying exponentials, hence convex and log-convex. For arbitrary two-branch geometries we have only computer-assisted ceilings.

Proposition 4.2 (Two-branch ceilings)**.** *For every $C \geq 1$ no two-branch state is entangled by the model at slab separation $d \geq 2.75\,\sigma$ (the branches of A and B on opposite sides of a plane, at normal distance $\geq d$), nor at closest approach $d \geq 3.78\,\sigma$.*

The inequalities that bound s are proven; the final maximisation over the two splittings is a floating-point evaluation without interval arithmetic, with a margin of 0.36% below $1/\sqrt{2}$ (Appendix B). A numerical search over all two-branch geometries found nothing above the closed forms of Table 1; we have not proven these to be the suprema. So at $C = 1$ the largest two-branch distance lies between $2.21\,\sigma$ and $2.75\,\sigma$ at slab separation, between $2.74\,\sigma$ and $3.78\,\sigma$ at closest approach, and equals $2.21\,\sigma$ within the parallel class.

4.2 Many branches: no critical distance

With many branches the condenser argument of Section 2 becomes a theorem: sheets of branches that are wide compared with the gap exceed any threshold below one.

Theorem 4.3 (No critical distance)**.** *For every $d > 0$ and every $C < \infty$ there are finite branch sets at slab separation d with $\rho_{\max} > s_*$. For uniform coaxial discs of radius a at gap d, each carrying a continuous uniform charge (or a point-branch lattice in the limit of spacing $\ll d$), each body carrying in addition a far copy of its disc, the far copies facing each other at gap d,*

$$\rho_{\max} \geq \operatorname{erf}(d/2\sigma)\Big(1 - \frac{3\pi d}{8a}\Big), \tag{13}$$

so the model entangles such states once $a/d > (3\pi/8)/(1 - s_*/\operatorname{erf}(d/2\sigma))$, which is 4.02 at $C = 1$ and $d \gg \sigma$. Sparse lattices can fall below (13).

The condition is on the extent of the coherent superposition in units of the gap, not on d/σ. The far copy is a second disc of branches, far from both near discs, on which the pattern has the opposite sign; the copy of B is the copy of A translated by d along the normal, so the two copies face each other at the same gap. It makes the pattern neutral without changing the correlation, and it means that the coherent extent of the state is really the distance to the copy (Section 5.3 gives the sharp extent law, also for a single sheet). Since $\rho_{\max} = 1$ for every pair of open supports (Remark 3.3), the absence of a critical distance is not by itself a physical prediction. What matters is how much entanglement the model can produce, and how fast.

5 The entangling rate against the model's own dephasing

5.1 The first-order rate

For equal masses write the rate (9) in units of the Newtonian rate, $\dot{\lambda} = -\kappa\, Gm^2/(\hbar d)$, with d the separation and $\kappa \geq 0$ dimensionless. Eq. (9) is also the initial rate when a local Hamiltonian is present [9]. The constant κ is bounded, because the coupling, of weight $\sqrt{1 + C^2}$, must first pay for the dephasing of its own witness, of weight C.

Theorem 5.1 (Rate bounds)**.** *Let $\theta = \min(1, s_*/\rho_{\max})$.*

(i) For every product state with closest approach d and every σ, $\kappa \leq (1 - \theta)\sqrt{1 + C^2}\, df(d) \leq \sqrt{1 + C^2} - C$.

(ii) For supports separated by a slab of width d, with the Coulomb kernel ($\sigma \to 0$),

$$\kappa \le B(C) = \sqrt{1+C^2} - C - C \ln \frac{\sqrt{1+C^2}}{C}, \tag{14}$$

which is 0.068 *at* $C = 1$ *and falls as* $1/(8C^3)$ *for* $C \to \infty$. *For planar supports at finite* σ *the corresponding bound is larger (Appendix C), so* (14) *is a statement for* $\sigma \ll d$.

The entangling rate is therefore a fraction of the Newtonian rate for every state, and a few per cent of it for slab-separated states at $\sigma \ll d$. Explicit states show how much of the bound can be reached. Give each mass an equal superposition of a planar sheet and a far copy of it, the two sheets facing each other at gap d and the two far copies likewise, in the formal limits $\sigma \to 0$ and zero thickness. A Gaussian sheet of the best width has $\kappa_G = 0.027$ at $C = 1$ (Eq. (27) in Appendix B). So at $C = 1$ and $\sigma \ll d$ the best rate constant of slab-separated states lies between 0.027 and 0.068. The lower end is a proven formula for one witness, in limits we do not control; at finite d/σ smearing raises both ends by corrections of first order in σ/d.

5.2 The ratio to the dephasing rate

The entangling rate has to be compared with the rate at which the same dynamics destroys the superpositions it acts on. The coherence between two branches a, a' of one body decays at the Diósi–Penrose rate $C\,Gm^2[f(0) - f(|a-a'|)]/\hbar$. Because the body is rigid and only its centre is delocalised, this saturates for $|a-a'|$ larger than a few $\sigma_{\rm eff}$:

$$\Gamma_{\rm sat} = \frac{C\,Gm^2 K_0}{\hbar}, \qquad K_0 = \frac{1}{\sqrt{\pi}\,\sigma_{\rm eff}}, \tag{15}$$

with $\sigma_{\rm eff} = \sigma$ for point masses and $K_0 = 6/(5R)$, $\sigma_{\rm eff} = 5R/(6\sqrt{\pi}) = 0.470\,R$, for uniform spheres of radius $R \gg \sigma$. A wide superposition does not dephase faster per pair. For extended bodies Theorem 3.2 and the bounds of this section hold verbatim with f replaced by the Coulomb energy $K(r)$ of two smeared bodies, which for $\sigma \ll R$ is $1/r$ beyond contact; at large separation only the self-term K_0 changes, and the radius takes the place of σ however small σ is. With $\Gamma_{\rm ent} = |\dot\lambda| = \kappa\,Gm^2/(\hbar d)$,

$$\mathcal{R} \equiv \frac{\Gamma_{\rm ent}}{\Gamma_{\rm sat}} = \frac{\kappa}{CK_0 d} = \frac{\sqrt{\pi}\,\kappa}{C}\,\frac{\sigma_{\rm eff}}{d}. \tag{16}$$

This is an identity, and its bounds are those of Theorem 5.1: the Newtonian rate falls as $1/d$ while the dephasing rate is fixed by the size of the body, and κ is small. At $C = 1$ the ratio is at most $0.12\,\sigma_{\rm eff}/d$ for slab-separated supports to leading order in σ/d (0.13 at $d = 10\,\sigma$ and 0.18 at $d = 3\,\sigma$ for planar supports; for other slab-separated supports at finite σ we have only the ceiling $0.73\,\sigma_{\rm eff}/d$ of Theorem 5.1(i)), and the best state known reaches $0.048\,\sigma_{\rm eff}/d$; at large C, $\mathcal{R} \le (\sqrt{\pi}/8C^4)\,\sigma_{\rm eff}/d$ (Fig. 2; Table 4 gives the dependence on C). As a function of the extent, $\mathcal{R}$ vanishes below a threshold, peaks near an extent of a few gaps, and falls off like gap over extent beyond: a wider sheet is not better.

The same dephasing is already inside the criterion, divided by the number of branches. The first term of the numerator of (9) is the Diósi–Penrose dephasing rate of the collective coherence that the witness reads. For a smooth pattern over n point-like branches its point self-energies $f_0 \sum |q(a)|^2$ are diluted as $1/n$, and to leading order the criterion $\rho_{\max} > s_*$ reads $n\,\mathcal{R}_{\rm coll} > 1$, where $n\mathcal{R}_{\rm coll} \equiv \xi = -\mu_{\min}/(Cf_0)$, with $\mu_{\min}$ the lowest eigenvalue of $Cf^\circ - \sqrt{1+C^2}\,F$ on

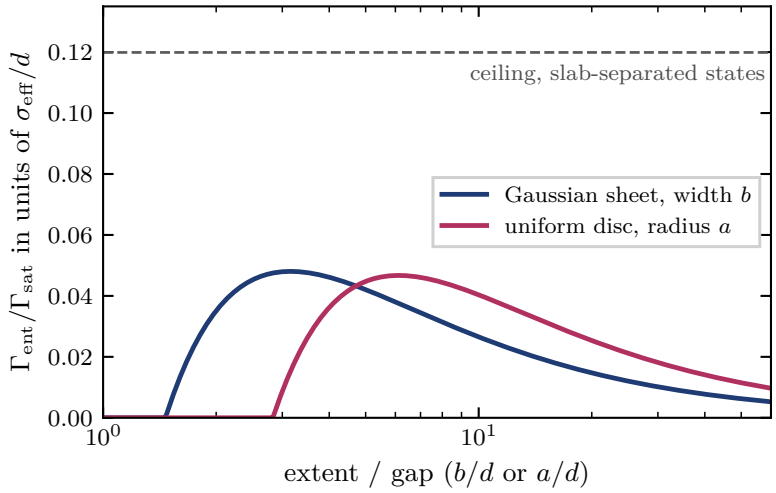


Figure 2. *Entangling rate over single-body dephasing rate, in units of $\sigma_{\rm eff}/d$, at $C = 1$, for a Gaussian sheet of rms width b and a uniform disc of radius a (each with a far copy, $\sigma \to 0$), against the extent in units of the gap. The dashed line is the ceiling (14) for all slab-separated states.*

the branch patch (f° the self-kernel f_A with its diagonal f_0 removed, F the cross kernel, unit-normalised patterns).

5.3 The extent law: how wide the superposition must be

For sheets the criterion is the electrostatics of a plate condenser. For coaxial discs of radius a at gap $d \gg \sigma$, each with a far copy, the copies facing each other at the same gap, the criterion becomes scale-free (formal limit $\sigma \to 0$, zero thickness). Writing the Hankel transform of an axisymmetric charge as an Abel transform, $\hat{q}(k) = \int_0^1 g(t)\cos(kt)\,dt$, turns the canonical correlation into the top eigenvalue of Love's operator for the circular plate condenser [15],

$$(T_\delta g)(t) = \frac{1}{\pi}\int_{-1}^{1} \frac{\delta\, g(s)}{\delta^2 + (t-s)^2}\,ds, \qquad \delta = d/a, \tag{17}$$

and the criterion is $\lambda_{\max}(T_{d/a}) > s_*$ (Appendix B, which also gives the condition (26) for the uniform pattern alone to be a witness). At $C = 1$ the coherent diameter must exceed about 5.5 gaps, with the far copy. On a single connected sheet the best pattern found is dipolar and needs a diameter of 14.8 gaps. The required extent grows like C^2 at large C. In a lattice with spacing larger than σ, the hexagonal and disc-shaped patches we examined reach the threshold with 10–15 d/σ point-like branches per mass at $d = 12$–$24\,\sigma$; we have not shown a lower bound. The thresholds, computed by converged Nyström discretisation of (17), are in Table 3, and the lattice counts in Appendix C.

5.4 The size of the entanglement

The rate bounds limit how fast entanglement starts. The next theorem limits how large it becomes. Below, the negativity is $|\lambda_{\min}(\rho_t^{T_1})|$, the quantity plotted in [9].

Theorem 5.2 (Negativity bound)**.** *For $H = 0$, equal masses, any product state with weights p,*

r on finite branch sets, θ as in Theorem 5.1, and all $t' = Gm^2 t/(\hbar\sigma) \geq 0$ (lengths in units of σ),

$$|\lambda_{\min}(\rho_t^{T_1})| \leq (1-\theta)\, t' \Big\{ \sum p_a p_{a'} r_b r_{b'} \, (C^2\delta^2 + \epsilon^2)\, e^{-2t'C\,(D_A + D_B + \min(\theta\delta,\delta))} \Big\}^{1/2}, \tag{18}$$

the sum over all a, a', b, b', with $\epsilon = F(a,b) - F(a',b')$. If the branches of each mass are at least ℓ apart, $D_\ell = f_0 - f(\ell) > f(d)$ and $C \geq 1/\sqrt{3}$, then $\sup_t |\lambda_{\min}| \leq (1-\theta)(f(d)/e)\big[1/(D_\ell - f(d)) + \sqrt{\sum p^2 + \sum r^2}/(CD_\ell)\big]$; for $\ell, d \gg \sigma$ and many branches this is at most $(\sqrt{\pi}/e)(1-s_*)\,\sigma/d$, which is $0.19\,\sigma/d$ at $C = 1$.

For many branches more than a few σ apart the entanglement is thus at most of order σ/d at all times, whatever the state. The proof (Appendix B) compares the model with a copy of itself whose cross kernel is weakened to θF, which is separable by Remark 3.1. For states with structure below σ the sum (18) has to be evaluated as it stands, and a σ/d bound for all product states is not proven.

A leading-order law. The bound lies well above what explicit states reach. Expanding the exact matrix elements to first order in the cross kernel, with the local dephasing kept exactly, gives an estimate of the actual size. For n branches per mass with uniform weights it is $n\lambda_{\min} \simeq e^{-2\tau}[e^{\tau} - 1 - \xi\tau]$ up to terms of relative order $1/n$, with $\tau = \Gamma_{\text{sat}} t$ and $\xi = n\mathcal{R}_{\text{coll}}$ the quantity whose exceeding one is the criterion. The factor $e^{-2\tau}$ is the survival of one coherence on each body, $e^{\tau} - 1$ the mixedness the dephasing creates in the witness subspace, $-\xi\tau$ the entangling term. For $\xi \gg 1$,

$$\lambda_{\min}(t) \simeq -\Gamma_{\text{ent}}\, t\, e^{-2\Gamma_{\text{sat}} t}, \qquad \max_t |\lambda_{\min}| \simeq \frac{\mathcal{R}}{2e} = \frac{\sqrt{\pi}}{2e}\,\frac{\kappa}{C}\,\frac{\sigma_{\text{eff}}}{d} \quad \text{at} \quad t_* = \frac{1}{2\Gamma_{\text{sat}}}. \tag{19}$$

The entanglement is what the entangling rate can build in half a dephasing time, so "negativity of order $10^{-2}\,\sigma_{\text{eff}}/d$", the value for Gaussian sheets at $C = 1$, is the statement that the entangling rate is a fraction of the dephasing rate, not an extra suppression. The law is derived; its error is not bounded. At $C = 1$ its finite-ξ form agrees to a few per cent with exact partial transposes of uniform lattice sheets at separations of $4\,\sigma$ and $6\,\sigma$; at $C = 2$ it overestimates the peak.

One explicit state shows both halves of the result (Appendix C). A sheet state with 38 branches per mass at slab separation $3.52\,\sigma$, beyond the two-branch ceiling of Proposition 4.2, is entangled, with an exact peak negativity of order 10^{-3}, against 0.41 for unitary Newtonian gravity on the same state.

6 The Bose *et al.* design and the inference from an observation

6.1 What the model predicts for the design

In the design of [1] the branches of A sit at 0 and 250 μm, those of B at 450 and 700 μm, collinear, with closest approach $d = 200$ μm and $m = 10^{-14}$ kg (a diamond sphere of radius $R = 0.879$ μm). This is a parallel two-branch configuration, so by Theorem 4.1 the model can entangle it only if σ is comparable to the separation. Eq. (11) gives the exact condition: $\sigma > 524$ μm at $C = 1$, and more at larger C (Table 3). With such a σ the model's force is no longer Newtonian at laboratory distances: at $\sigma = 524$ μm the smeared force between two point masses 1 mm apart is 0.39 of its Newtonian value, and torsion-balance tests of the inverse-square

law at such separations show no deviation at that level [16]. Other two-branch geometries at the same closest approach lower the threshold on σ only to some tens of micrometres (Appendix C).

Many-branch states at the same separation can be entangled for any σ, but only at the rates of Section 5. For $\sigma \ll R$ and $C = 1$ each body dephases at $\Gamma_{\mathrm{sat}} = 86\ \mathrm{s}^{-1}$, while the best sheet state known entangles at $\Gamma_{\mathrm{ent}} = 8.6 \times 10^{-3}\ \mathrm{s}^{-1}$: the superposition is lost about ten thousand times faster than entanglement builds up. By the law (19) the negativity then peaks at order 10^{-5}, half a dephasing time after preparation (Appendix C).

6.2 What an observed entanglement excludes

An observed entanglement can still exclude the model, through the geometry of the state or the size and time course of the signal, but not through the separation alone.

Remains true. (i) Two-branch states with ideal branches are not entangled by the model at any time unless the separation is comparable to σ: at $C = 1$, below $2.21\,\sigma$ for parallel superpositions (Theorem 4.1) and below $2.75\,\sigma$ at slab separation for any two-branch geometry (Proposition 4.2, computer-assisted). For the design above, with ideal branches, a positive result of the expected size excludes the model for every σ below 524 μm. (ii) For any state of many branches that are more than a few σ apart, the negativity at $C = 1$ stays below $0.19\,\sigma_{\mathrm{eff}}/d$ when the branch spacing and d are much larger than σ (the proven bound is $0.23\,\sigma/d$ at $d = 10\,\sigma$ and $0.43\,\sigma/d$ at $d = 3\,\sigma$; Theorem 5.2), against about 0.4 for unitary gravity. An entanglement signal of the size the quantum prediction gives, or one that oscillates or persists beyond a few dephasing times $1/\Gamma_{\mathrm{sat}}$, is incompatible with the model. (iii) Before entanglement is at issue, the survival of each body's superposition over the experiment already tests the model.

No longer true. (i) "The Diósi–Penrose dynamics cannot entangle masses further apart than $0.85\,\sigma$ (or $2.21\,\sigma$)", read as a statement about the model. It is a statement about particular two-branch geometries. The same applies to "the dynamics is separability-preserving for $d \gg \sigma$". (ii) The geometry-free inference "any entanglement detected beyond $2.2\,\sigma$ falsifies the model, whatever the state and whatever its size".

Not decided. For wavepackets of finite width the criterion is degenerate (Remark 3.3): every such state is entangled at once, and we give no bound on how much. The design therefore excludes the model for a result of the expected size, not for any positive result.

7 Scope and discussion

Position-eigenstate branches. Theorem 3.2 is exact for branches that are position eigenstates. For wavefunctions whose support has interior the yes/no question has no content (Remark 3.3); Theorem A.1 gives the entangling direction, with the rate (9) in integral form. The negativity bound (18) is proven for finite branch sets only; we give none in terms of the packet width.

The kinetic term. All results are for $H = 0$. The initial rate (9) and the bounds of Theorem 5.1 are unchanged by any local Hamiltonian defined on the initial state, and local Hamiltonians acting within a finite set of sites cannot make a sub-threshold region entangling (Theorem 3.2(b)). Beyond that we control nothing: free packets acquire full support at once, and the negativity bound has not been extended to them. For $m = 10^{-14}$ kg the relevant experiments sit deep in the static regime, which is an argument, not a bound.

Preparation. Every result assumes the product state exists at $t = 0$. The same dephasing acts

while it is made: a superposition over some 10–15 d/σ positions in the lattice patches examined, more than five gaps across, must be made in a time short compared with $1/\Gamma_{\mathrm{sat}}$ (11.6 ms for the mass above).

Superpositions smaller than σ. The rate ratio (16), the σ/d bounds and the law (19) assume branches further apart than σ_{eff}, which dephase at Γ_{sat}. Figure 3 of [9] is in the other regime: superposition size $L = 23$ μm, $d = 24$ μm, $m = 10^{-15}$ kg and $\sigma = 50$–250 μm, so that $L, d < \sigma$. Theorem 3.2, the rate bound of Theorem 5.1(i) and the bound (18) hold there exactly. At $C = 1$ the pair of branches dephases at $\Gamma_L = Gm^2[f_0 - f(L)]/\hbar$, with $1/\Gamma_L \simeq (12\,\sigma^2/L^2)/\Gamma_{\mathrm{sat}}$; for collinear superpositions at this closest approach the entanglement peaks at half to two thirds of that time and lasts from 8 h at $\sigma = 75$ μm to 23 days at $\sigma = 250$ μm, and it is not small, because $d < \sigma$.

What is numerical. The critical distances, the constants Λ_+, $L_{1/2}$, the extent thresholds and the rate constants are roots and maxima of explicit one-dimensional functions, or top eigenvalues of converged discretisations of Love's operator (Appendix C). Proposition 4.2 is computer-assisted, in floating point, without interval arithmetic. That the closed forms of Table 1 are the two-branch suprema over all geometries rests on numerical search. On discs, the optimality of the axisymmetric sector and of the dipolar pattern on a single disc is numerical. The leading-order law (19) is derived without an error bound and was compared with exact partial transposes of lattice sheets only.

Also open. Separability after the negative eigenvalue has returned to zero; the best rate constant, between 0.027 and 0.068 at $C = 1$; non-planar supports; noise kernels other than the Newtonian one; $C < 1$, which is not a classical model; the unsmeared-force variant, which is not a measurement-and-feedback model and to which the pair decomposition does not apply.

Discussion. The Diósi–Penrose model is a classical channel with a definite structure: one kernel in force and noise, and a local dephasing equal to the Gram form of that kernel. That structure gives an exact criterion, a canonical correlation against $C/\sqrt{1+C^2}$, which answers the question of [9]. The model can in principle produce entanglement at any separation, with many branches spread coherently over several times the separation. Its generator is not separability-preserving at any distance, so it is not a local-operations-and-classical-communication channel, and a critical distance is a property of a two-branch geometry, not of the model. But it produces entanglement at a rate of order σ_{eff}/d times the rate at which it destroys the superposition itself, and for branches more than a few σ apart the entanglement never exceeds a fraction of order σ_{eff}/d of what unitary gravity gives. For entanglement-witness experiments the discriminants are the size and time course of the signal and, before them, the survival of the single-body superposition. The separation alone discriminates only for two-branch states.

Appendix A: Proof of the separable half, and wavefunctions

Proof of Theorem 3.2(b). Absorb the masses into g. Choose orthonormal bases e_i of V_A and e'_i of V_B with $\langle e_i, e'_j\rangle = s_i\delta_{ij}$ (singular value decomposition; $s_1 = \rho_{\max}$, $s_i = 0$ beyond the smaller rank). Fix reference branches a_0, b_0 and put $x_i(a) = \langle e_i, g_a - g_{a_0}\rangle$, $y_i(b) = \langle e'_i, g_b - g_{b_0}\rangle$. Since the $g_a - g_{a'}$ lie in V_A,

$$D_A = \tfrac{1}{2}\sum_i \big(x_i(a) - x_i(a')\big)^2, \qquad \delta = \sum_i s_i\big(x_i(a) - x_i(a')\big)\big(y_i(b) - y_i(b')\big), \tag{20}$$

and $F(a,b) = \sum_i s_i x_i(a) y_i(b) + \varphi_A(a) + \varphi_B(b) + \text{const}$. Hence $\Lambda = \sum_i \Lambda_i + i[\varphi_A(a) - \varphi_A(a')] + i[\varphi_B(b) - \varphi_B(b')]$ with Λ_i as in Eq. (10); the phases φ are local unitaries. For each i take real Gaussian variables $(\eta_i, \zeta_i, \eta_i', \zeta_i')$, mean zero, independent for different i, with covariance

$$t\, s_i \begin{pmatrix} |J| & J \\ J & |J| \end{pmatrix}, \qquad J = \begin{pmatrix} 0 & \frac{1}{2} \\ \frac{1}{2} & C \end{pmatrix}, \tag{21}$$

positive semidefinite because $|J| \pm J \geq 0$. Define the random diagonal operators $U_A = \sum_a \exp[\sum_i x_i(a)(\eta_i + i\zeta_i)]\, |a\rangle\langle a|$ and U_B likewise with y_i, η_i', ζ_i'. With $\mathbb{E}\, e^Z = e^{\mathbb{E}[Z^2]/2}$ the cross covariances $\mathbb{E}[\zeta_i \zeta_i'] = t s_i C$ and $\mathbb{E}[\eta_i \zeta_i'] = \mathbb{E}[\zeta_i \eta_i'] = t s_i/2$ give

$$\begin{aligned} &\mathbb{E}\big[u_A(a) u_B(b) \bar{u}_A(a') \bar{u}_B(b')\big] \\ &\quad = \exp\Big\{ t \sum_i s_i \big[i(x_i y_i - x_i' y_i') - C(x_i - x_i')(y_i - y_i') \big] \Big\}\, L_A(a,a') L_B(b,b'), \end{aligned} \tag{22}$$

using $(x + x')(y - y') + (x - x')(y + y') = 2(xy - x'y')$, with local factors L. Dividing, $e^{t\Lambda} = \mathbb{E}[u\bar{u}]\, T_A(a,a') T_B(b,b')$ up to the local phases, with

$$T_A(a,a') = d(a)\overline{d(a')}\, \exp\Big\{ t \sum_i \big(C - s_i \operatorname{tr}|J|\big) x_i(a) x_i(a') \Big\}, \qquad \operatorname{tr}|J| = \sqrt{1 + C^2}, \tag{23}$$

d a non-vanishing diagonal factor, and the same for T_B. If $s_i\sqrt{1+C^2} \leq C$ for all i the exponent is t times a positive semidefinite matrix; its entrywise exponential is positive semidefinite by the Schur product theorem [17], so T_A and T_B act as completely positive Schur multipliers $\mathcal{T}_A$, $\mathcal{T}_B$. Therefore

$$\rho_t = \mathbb{E}\Big[(U_A \otimes U_B)\, (\mathcal{T}_A \otimes \mathcal{T}_B)(\rho_0)\, (U_A \otimes U_B)^\dagger \Big], \tag{24}$$

a mixture of products of local completely positive maps, trace preserving in total because the diagonal of $e^{t\Lambda}$ is one. Separable states go to separable states. Interleaved local channels and the Lie–Trotter limit in finite dimension, with the separable set closed, give the last statement. The construction needs only that the Gram matrices f_A, f_B are non-singular (distinct branches); it holds for any number of branches, any amplitudes and every $t \geq 0$. If $\rho_{\max} > s_*$, then T_A and T_B are indefinite and part (a) shows the state entangled. □

Dictionary for Remark 3.2. Each Λ_i in Eq. (10) is the generator of Lemma 3 of [12] with $O_A = \sum_a x_i(a)|a\rangle\langle a|$, $O_B = \sum_b y_i(b)|b\rangle\langle b|$, coupling $\lambda = -s_i$, local rates $\Gamma_A = \Gamma_B = C$ and cross rate $\Gamma_{AB} = -C s_i$ (in units $Gm^2/\hbar\sigma$). Their lemma makes $e^{t\Lambda_i}$ separable when $\lambda^2 + \Gamma_{AB}^2 \leq \Gamma_A \Gamma_B$, which is $s_i\sqrt{1+C^2} \leq C$.

Wavefunctions. For wavefunctions only the entangling half of the criterion survives: a witness with bounded patterns, on regions where the wavefunctions do not vanish, makes the state entangled at once.

Theorem A.1 (Wavefunctions, entangling direction)**.** *Let $\psi_A, \psi_B \in L^2(\mathbb{R}^3)$ and $H = 0$. Suppose there are bounded neutral q_1, q_2, supported on sets of finite measure on which $|\psi_A|, |\psi_B| \geq \varepsilon > 0$, with $C\langle q_1, q_1\rangle + C\langle q_2, q_2\rangle - 2\,\mathrm{Re}[(C+i)\langle q_1, q_2\rangle] < 0$ in the smeared Coulomb form. Then ρ_t is entangled for all sufficiently small $t > 0$.*

Proof. The kernel Λ is bounded ($|f| \le f_0$). With $c = q_1 \otimes |\psi_B|^2 + |\psi_A|^2 \otimes q_2 \in L^1$ and $\chi = c/\tilde{\Psi}^* \in L^2$, $\langle\chi|\rho_t^{T_1}|\chi\rangle = \iint \bar{c}\, c\, e^{t\Lambda} = t\,(\text{negative}) + O(t^2\|c\|_1^2)$. A separable state has a positive partial transpose, whose quadratic form is non-negative. □

Since the smeared point charges of any open set span the Coulomb space (their potentials are real-analytic), such q_1, q_2 exist for every pair of supports with interior and every separation.

Appendix B: Proofs of the bounds

Lengths are in units of σ unless stated.

Proof of Theorem 4.1. $h(x) = f(\sqrt{x}) = \pi^{-1/2}\int_0^1 e^{-xu^2/4}du$ is a mixture of decaying exponentials: decreasing, convex and log-convex. Put $x = |r|^2$, $y = |w|^2$, $P = |r-w|^2$, $Q = |r+w|^2$, so $P+Q = 2x+2y$, and $N = 2h(x) - h(P) - h(Q)$, $s = |N|/(2D(|w|))$. If $N > 0$: convexity gives $h(P)+h(Q) \ge 2h(x+y)$, log-convexity $h(x+y)h(0) \ge h(x)h(y)$, so $N \le 2[h(x) - h(x+y)] \le 2(f(|r|)/f_0)\, D(|w|)$, and $|r| \ge d$. If $N < 0$: (i) $-N$ is the second difference of $t \mapsto f(|r+tw|)$ at $t = -1, 0, 1$, hence $\le |w|^2\Lambda_+$, with Λ_+ the largest Hessian eigenvalue of f over space, which is $\max f''$ because $f' < 0$; (ii) with $P \le Q$ the parallelogram law gives $Q \ge x$, so $-N \le h(P) - h(x) \le f(d)$. For $|w| \ge L_{1/2}$, (ii) gives $-N/(2D) \le f(d)/f_0$. For $|w| \le L_{1/2}$, (i) gives $-N/(2D) \le \Lambda_+|w|^2/(2D(|w|)) \le \Lambda_+ L_{1/2}^2/f_0$, because $L^2/D(L)$ is increasing ($D(L)/L^2$ is a difference quotient of the convex h). The transversal family with $L \to \infty$ approaches $f(d)/f_0$ from below. □

Proof of Proposition 4.2. Write $N = \psi(b_1) - \psi(b_2)$ with $\psi(b) = f(|b-a_1|) - f(|b-a_2|)$. (i) $|\psi| \le g_d L_A$ with $g_d = \sup_{r\ge d}|f'|$. (ii) $|\psi| \le m_d(L_A)$, $m_d(L) = \sup_{r\ge d}[f(r) - f(r+L)]$. The same with A and B exchanged. (iii) N is a double difference, so $|N| \le L_A L_B \sup\|\nabla^2 f\|$ over the parallelogram of difference vectors, on which $|x| \ge d$ at slab separation and $|x| \ge d - (L_A+L_B)/2$ at closest approach; $\|\nabla^2 f\| = \max(|f''|, |f'|/r) \le \kappa_0$. Then

$$s \le \frac{\min\{2g_dL_A,\, 2g_dL_B,\, 2m_d(L_A),\, 2m_d(L_B),\, HL_AL_B\}}{2\sqrt{D(L_A)D(L_B)}}, \tag{25}$$

with H the supremum in (iii), maximised over (L_A, L_B) with cell bounds (numerators at the upper corner, denominators at the lower corner of each cell of a geometric grid of ratio 1.01, a last cell for $L > 400\,\sigma$), using that $L/\sqrt{D(L)}$, m_d and D are monotone. The suprema over r are taken on grids, and the whole evaluation is in floating point without interval arithmetic. The bound is non-increasing in d. It is 0.70456 at $2.75\,\sigma$ (slab) and 0.70457 at $3.78\,\sigma$ (closest approach), 0.36% below $1/\sqrt{2}$, and exceeds $1/\sqrt{2}$ at $2.735\,\sigma$ (0.70875) and $3.765\,\sigma$ (0.71019). □

The numerical search over two-branch geometries. Differential evolution followed by Nelder–Mead, over several parametrisations of the two branch pairs with the separation constraint built in, found nothing above $f(d)/f_0$ at slab separation, or above $\max(f(d)/f_0, \text{straddle limit})$ at closest approach. This supports, but does not prove, that the closed forms of Table 1 are the suprema over all two-branch geometries.

Proof of Theorem 4.3. Smearing lowers the self-energy, so $\langle q, q\rangle \le 16/(3\pi a)$ per unit-charge uniform disc; $f(r) \ge \operatorname{erf}(d/2\sigma)/r$ for $r \ge d$; and for unsmeared coaxial discs $E(0) - E(d) = \int \frac{d^2k}{(2\pi)^2}\frac{2\pi}{k}|\hat{q}|^2(1-e^{-kd}) \le 2\pi d \int q^2 = 2d/a^2$. The far copies, which face each other at the same gap, make the pattern neutral without changing the ratio; this proves (13). For the first statement at arbitrary d and C, let A carry a uniform planar lattice patch (with in-plane distances $\Delta_{jj'}$) and its far copy, and B the same patch and far copy translated by d along the normal. The same Fourier estimate, with the smeared kernel, gives $1-\rho_{\max} \le (d/2\sigma^2)\sum_{jj'} e^{-\Delta_{jj'}^2/4\sigma^2} / \sum_{jj'} f(\Delta_{jj'})$; the numerator grows like the number of points and the denominator like its square times f of the patch size, so the right side tends to zero for growing patches. As wavefunctions, discs of small thickness inherit a strict inequality by continuity of the bounded smeared kernel. □

Derivation of the extent law. For charges on coaxial unit discs at gap δ ($\sigma \to 0$), the mutual energy is, up to a common constant, $E(\delta) = \int_0^\infty e^{-k\delta}\hat{q}(k)^2 dk$, with $\hat{q}$ the Hankel transform of the charge. Writing an axisymmetric charge through its Abel transform, $\hat{q}(k) = \int_0^1 g(t)\cos(kt)\,dt$ with g extended evenly to $(-1,1)$, gives $E(0) = (\pi/2)\int_0^1 g^2$ and $E(\delta) = (\pi/2)\int_0^1 g\,T_\delta g$, with T_δ of Eq. (17), the operator of Love's integral equation [15]. The canonical correlation is the top eigenvalue of T_δ on even functions. The uniform disc is $g(t) = \sqrt{1-t^2}$. Its Rayleigh quotient is $\Phi(a/d)$, so the uniform pattern is a witness if and only if

$$\Phi(a/d) > s_*, \qquad \Phi(x) = \frac{3\pi}{16}\int_0^\infty \Big(\frac{2J_1(u)}{u}\Big)^2 e^{-u/x}\,du. \tag{26}$$

Proof of Theorem 5.1. (i) $C\langle q_1,q_1\rangle + C\langle q_2,q_2\rangle \ge 2C|\langle q_1,q_2\rangle|/\rho_{\max}$, so the numerator of (9) is $\ge -2(1-\theta)\sqrt{1+C^2}|\langle q_1,q_2\rangle|$, and $|\langle q_1,q_2\rangle| \le f(d)\|q_1\|_1\|q_2\|_1 \le \frac{1}{2}f(d)(\sum|q_1|^2/p + \sum|q_2|^2/r)$ by Cauchy–Schwarz. (ii) For charges at depths $z \le 0$ and $z' \ge d$, $\langle q_1,q_2\rangle = \int \frac{d^2k}{(2\pi)^2}\frac{2\pi}{k}e^{-kd}\bar{A}_1 A_2$ with $A_1(k) = \int dz\, e^{kz}\hat{q}_1(k,z)$, $|A_1| \le \|q_1\|_1$, and $\langle q_1,q_1\rangle \ge \int \frac{d^2k}{(2\pi)^2}\frac{2\pi}{k}|A_1|^2$, because $e^{-k|z-z'|} - e^{k(z+z')}$ is $2k$ times the Dirichlet Green function of $-\partial_z^2 + k^2$ on the half-line, a positive kernel. Then mode by mode the numerator is at least $-\int \frac{d^2k}{(2\pi)^2}\frac{2\pi}{k}[\sqrt{1+C^2}e^{-kd} - C]_+(|A_1|^2 + |A_2|^2)$, and $\int_0^\infty [\sqrt{1+C^2}e^{-kd} - C]_+ dk = B(C)/d$. With smearing, for planar supports, e^{-kz} is replaced by $w(k,z) = \frac{1}{2}[e^{-kz}\operatorname{erfc}(\sigma k - z/2\sigma) + e^{kz}\operatorname{erfc}(\sigma k + z/2\sigma)]$, which gives the finite-σ value of Table 2. □

Gaussian sheets. For the explicit states of Section 5, a Gaussian sheet of rms width b facing the sheet of the other mass at gap d ($\sigma \to 0$, zero thickness), the same mode formula gives the rate of the witness proportional to the sheet profile. Maximised over the width, it is

$$\kappa_G = \max_y \frac{\sqrt{\pi}}{2}\, y\big[\sqrt{1+C^2}\, e^{y^2}\operatorname{erfc}(y) - C\big], \qquad y = \frac{d}{2b}. \tag{27}$$

Proof of Theorem 5.2. Let Λ_θ be Λ with F replaced by θF in the Hamiltonian and in the correlated noise, local dephasing unchanged, and $\rho_t^\theta = \rho_0 \circ e^{t'\Lambda_\theta}$. Its canonical correlations are $\theta s_i \le s_*$, so by Remark 3.1 ρ_t^θ is separable and $(\rho_t^\theta)^{T_1} \ge 0$. Now $\rho_t = \rho_t^\theta \circ M$ with $M = \exp[t'(1-\theta)(i\epsilon - C\delta)]$, so by Weyl's inequality $\lambda_{\min}(\rho_t^{T_1}) \ge -\|\rho_t^\theta \circ (M-1)\|_{\mathrm{HS}}$, the Hilbert–Schmidt norm being invariant under partial transposition. Entrywise $|\rho_t^\theta| = (p_a p_{a'} r_b r_{b'})^{1/2} e^{-t'C(D_A + D_B + \theta\delta)}$ and $|M-1| \le t'(1-\theta)(\epsilon^2 + C^2\delta^2)^{1/2}\max(1, e^{-t'(1-\theta)C\delta})$; every exponent is non-positive since $D_A + D_B + \delta = \frac{1}{2}\|g_a - g_{a'} + g_b - g_{b'}\|^2 \ge 0$. For the corollary: terms with $a \ne a'$, $b \ne b'$ have

$C^2\delta^2 + \epsilon^2 \le 4C^2 f(d)^2$ (for $C \ge 1/\sqrt{3}$) and exponent $\ge 2D_\ell - 2f(d)$; terms with one index pair equal have $\delta = 0$, $|\epsilon| \le f(d)$, exponent $\ge D_\ell$ and weight $\sum p^2$ or $\sum r^2$; and $\sup_t te^{-\alpha t} = 1/(e\alpha)$. For $\ell, d \gg \sigma$, $D_\ell \to f_0 = 1/\sqrt{\pi}$ and $\sum p^2, \sum r^2 \to 0$. □

Appendix C: Numerical values

This appendix collects the precise values behind the rounded numbers of the main text. Lengths are in units of σ unless stated, and point masses are assumed except where σ_{eff} appears. Every entry is a root, a maximum or a top eigenvalue of a formula stated in the text.

Table 2. *Constants that enter the theorems, the rate bounds and the estimates of the main text, with the place where each is used. Values are at $C = 1$ unless stated.*

quantity	where	value
$\Lambda_+ = \max f''$	Theorem 4.1	$0.311326\,\kappa_0$, at $r = 3.2273\,\sigma$
$L_{1/2}$, $f(L_{1/2}) = f_0/2$	Theorem 4.1	$3.497418\,\sigma$
$c_* = \Lambda_+ L_{1/2}^2/f_0$	Theorem 4.1	0.634687; $s_*(C) \ge c_*$ for $C \ge 0.8213$
straddle above transversal	Table 1	for $d < 3.699\,\sigma$, i.e. every $C > 0.5396$
sufficient extent, uniform discs	Theorem 4.3	$a/d > 4.022$ ($d \gg \sigma$)
κ, any product state	Theorem 5.1(i)	$\le \sqrt{2} - 1 = 0.4142$
slab ceiling $B(1)$	Eq. (14)	0.067640
planar ceiling at $d = 3\,\sigma$ (finite σ)	Appendix B	0.104
Gaussian sheets κ_G	Eq. (27)	0.027108 at $b = 3.15\,d$; zero for $b/d \le 1.465$
uniform disc, uniform witness	Fig. 2	$\kappa = 0.0264$ at $a = 6.12\,d$
$1/\mathcal{R}$, slab ceiling; Gaussian sheets	Eq. (16)	$8.3\,d/\sigma_{\text{eff}}$; $20.8\,d/\sigma_{\text{eff}}$
negativity bound, $\ell, d \gg \sigma$	Theorem 5.2	$0.191\,\sigma/d$; $0.069\,\sigma/d$ at $C = 2$
peak by the law, Gaussian sheets	Eq. (19)	$8.8 \times 10^{-3}\,\sigma_{\text{eff}}/d$
peak by the law, slab ceiling	Eq. (19)	$2.2 \times 10^{-2}\,\sigma_{\text{eff}}/d$

Table 3. *Dependence on the noise strength C. Two-branch critical distances (in units of σ) of the transversal ($L \to \infty$) and straddle families; the threshold on σ above which the design of [1] is entangled; and the smallest a/d for which discs of radius a at gap d (each with a far copy, $\sigma \ll d$) are entangled, for the uniform pattern, Eq. (26), and the optimal axisymmetric pattern, Eq. (17).*

C	transversal	straddle	design, $\sigma >$	uniform pattern	optimal pattern
1	2.2109	2.7381	524.494 μm	2.8316	2.7706
1.25	1.8203	2.4425	617 μm	4.1316	4.0642
2	1.1845	1.9106	910 μm	9.7539	9.6453
5	0.4870	1.1832	2158 μm	58.810	58.041

Table 4. *The ratio $\mathcal{R} = \Gamma_{\text{ent}}/\Gamma_{\text{sat}}$ in units of σ_{eff}/d. The first column is the Gaussian sheet of Eq. (27) ($\sigma \to 0$, zero thickness); the second the slab bound (14) ($\sigma \ll d$); the third Theorem 5.1(i), any product state, any σ.*

C	Gaussian sheets	slab-separated, ceiling	any product state, ceiling
1	0.0481	0.120	0.734
1.25	0.0235	0.0590	0.497
2	0.00453	0.0115	0.209
5	0.000135	0.00034	0.035

Extent. At $C = 1$ the optimal pattern needs a coherent diameter of 5.54 gaps, the uniform one 5.66. At large C, $1 - \Phi \simeq (3\pi/8)\, d/a$ gives $a/d \simeq (3\pi/4)C^2 = 2.356\, C^2$ for the uniform pattern. Without the far copy, the best neutral pattern found on a single disc is dipolar, the odd block of Love's operator: it needs $a/d > 7.390$, a coherent diameter of 14.8 gaps, against $a/d > 11.34$ (22.7 gaps) for the best axisymmetric neutral pattern. For lattice patches with a far copy at $C = 1$, the far copies facing each other at gap d, the smallest number of point branches per mass that reaches the threshold is 182 ($15.2\, d/\sigma$) at $d = 12\,\sigma$ and 338 ($14.1\, d/\sigma$) at $d = 24\,\sigma$ for hexagonal patches, and 126 ($10.5\, d/\sigma$) and 316 ($13.2\, d/\sigma$) for disc-shaped cuts of the hexagonal lattice, with spacing and radius optimised; the best spacing is comparable to d.

The leading-order law at finite ξ. From $n\lambda_{\min} \simeq e^{-2\tau}[e^{\tau} - 1 - \xi\tau]$, n times the peak is $\xi/2e - 0.239 + O(1/\xi)$, and it vanishes at $\xi = 1$.

An explicit state. Take for each mass a hexagonal patch of 19 point branches with spacing $8\,\sigma$, plus its far copy (38 branches per mass), the two patches facing each other at slab separation $d = 3.52\,\sigma$ and the two far copies likewise, and $C = 1$. Then $\rho_{\max} = 0.813 > s_*$, $\kappa = 0.0258$, $\mathcal{R} = 0.0130$ and $\mathcal{R}/2e = 2.4 \times 10^{-3}$. Exact diagonalisation of the 1444-dimensional partial transpose gives a smallest eigenvalue of -1.6×10^{-3} at $t' = 0.5$, when each body's coherence is still 0.75; the peak lies below the large-ξ value because this state is sparse. Unitary Newtonian gravity ($1/r$ coupling, no noise) on the same state reaches -0.41.

The design of [1]. At $C = 1$ the two-branch threshold is $\sigma > 524.494$ μm. No two-branch geometry with closest approach 200 μm is entangled unless $\sigma > 73.0$ μm (straddle) or 90.5 μm (slab), according to the numerical suprema of Section 4; Proposition 4.2 guarantees $\sigma > 52.9$ μm (any geometry) or 72.7 μm (slab). For $\sigma \ll R$ and $C = 1$ the coherence time is $1/\Gamma_{\text{sat}} = 11.6$ ms, and over the 2.5 s of the proposed experiment the dephasing exponent is 216; over the same time unitary Newtonian gravity gives the two-branch design an entangling phase of 0.314 rad. The best Gaussian sheet at $d = 200$ μm has $b \approx 630$ μm, $\mathcal{R} = 9.9 \times 10^{-5}$, and by Eq. (19) a peak negativity of 1.8×10^{-5} at 5.8 ms.

References

[1] S. Bose, A. Mazumdar, G. W. Morley, H. Ulbricht, M. Toroš, M. Paternostro, A. A. Geraci, P. F. Barker, M. S. Kim, and G. Milburn, *Spin Entanglement Witness for Quantum Gravity*, Phys. Rev. Lett. **119**, 240401 (2017). doi:10.1103/PhysRevLett.119.240401

[2] C. Marletto and V. Vedral, *Gravitationally Induced Entanglement between Two Massive Particles is Sufficient Evidence of Quantum Effects in Gravity*, Phys. Rev. Lett. **119**, 240402 (2017). doi:10.1103/PhysRevLett.119.240402

[3] L. Diósi, *A universal master equation for the gravitational violation of quantum mechanics*, Phys. Lett. A **120**, 377 (1987). doi:10.1016/0375-9601(87)90681-5

[4] L. Diósi, *Models for universal reduction of macroscopic quantum fluctuations*, Phys. Rev. A **40**, 1165 (1989). doi:10.1103/PhysRevA.40.1165

[5] R. Penrose, *On gravity's role in quantum state reduction*, Gen. Relat. Gravit. **28**, 581 (1996). doi:10.1007/BF02105068

[6] A. Tilloy and L. Diósi, *Sourcing semiclassical gravity from spontaneously localized quantum matter*, Phys. Rev. D **93**, 024026 (2016). doi:10.1103/PhysRevD.93.024026

[7] A. Tilloy and L. Diósi, *Principle of least decoherence for Newtonian semiclassical gravity*, Phys. Rev. D **96**, 104045 (2017). doi:10.1103/PhysRevD.96.104045

[8] D. Kafri, J. M. Taylor, and G. J. Milburn, *A classical channel model for gravitational decoherence*, New J. Phys. **16**, 065020 (2014). doi:10.1088/1367-2630/16/6/065020

[9] D. Trillo and M. Navascués, *The Diósi–Penrose model of classical gravity predicts gravitationally induced entanglement*, Phys. Rev. D **111**, L121101 (2025). doi:10.1103/PhysRevD.111.L121101

[10] O. Angeli and M. Carlesso, *Entanglement in Markovian hybrid classical-quantum theories of gravity*, Phys. Rev. D **112**, 024047 (2025). doi:10.1103/jzht-fbwt

[11] A. Di Biagio, *Gravity-induced entanglement is not a theory-independent witness of nonclassicality of the gravitational field*, arXiv:2511.02683 (2025). arXiv:2511.02683

[12] Y.-X. Wang, J. S. Pedernales, and M. B. Plenio, *Recoverability of Gravitational Entanglement under Decoherence*, arXiv:2611.05044 (2026). arXiv:2611.05044

[13] H. Hotelling, *Relations Between Two Sets of Variates*, Biometrika **28**, 321 (1936). doi:10.1093/biomet/28.3-4.321

[14] A. Peres, *Separability Criterion for Density Matrices*, Phys. Rev. Lett. **77**, 1413 (1996). doi:10.1103/PhysRevLett.77.1413

[15] E. R. Love, *The Electrostatic Field of Two Equal Circular Co-axial Conducting Disks*, Q. J. Mech. Appl. Math. **2**, 428 (1949). doi:10.1093/qjmam/2.4.428

[16] J. G. Lee, E. G. Adelberger, T. S. Cook, S. M. Fleischer, and B. R. Heckel, *New Test of the Gravitational $1/r^2$ Law at Separations down to 52 μm*, Phys. Rev. Lett. **124**, 101101 (2020). doi:10.1103/PhysRevLett.124.101101

[17] R. A. Horn and C. R. Johnson, *Matrix Analysis*, 2nd ed. (Cambridge University Press, 2013). ISBN 9780521839402.